Eur. Phys. J. B **49**, 67–75 (2006)
DOI: 10.1140/epjb/e2006-00031-3

THE EUROPEAN PHYSICAL JOURNAL B

Band structure and high pressure study of Rh_3Sc, Rh_3Y and Rh_3La

M. Sundareswari[1] and M. Rajagopalan[2,a]

[1] Department of Physics, Sathyabama Deemed University, Chennai, India
[2] Department of Physics, Anna University, Chennai, India

Received 12 November 2005
Published online 31 January 2006 –

Abstract. The electronic structure of the Rhodium based intermetallic compounds (A_3B) such as Rh_3Sc, Rh_3Y and Rh_3La are studied by the Self Consistent Tight Binding Linear Muffin Tin Orbital (TB-LMTO) method. In the present work, an attempt has been made to understand why the compounds namely Rh_3Y and Rh_3La crystallize in hexagonal structure, rather than the cubic structure, where as some of the similar rhodium based A_3B compounds namely Rh_3Ti, Rh_3Zr, Rh_3Hf, Rh_3V, Rh_3Nb, Rh_3Ta and Rh_3Sc are found to stabilize in cubic structure. In this work a prediction has been made about the structural phase transition in Rh_3Y and Rh_3La, from Hexagonal phase to Cubic phase. A report of the lattice constant, bulk moduli, cohesive energy and electronic specific heat coefficient is made and is compared with the available experimental data. Band structure and density of states histograms are also plotted. An electronic topological transition is predicted in Rh_3La, which may lead to the changes in the Fermi surface topology and hence changes the physical properties of Rh_3La.

PACS. 71.20.-b Electron density of states and band structure of crystalline solids – 71.15.Mb Density functional theory, local density approximation, gradient and other corrections – 71.20.Lp Intermetallic compounds

1 Introduction

Recent developments in materials processing suggest that intermetallics may be useful in structural applications where ceramics are now contemplated for use. Further numerous non-structural applications that exploit the electrical, thermal, magnetic and corrosion properties of intermetallics have also been identified. Conventionally it is the nickel based single crystal alloys which find applications in gas turbine engines; but their applications in turbine blades and vanes of modern aero engines are limited at high temperatures, due to their low melting point (∼1450 °C). Hence it becomes necessary to develop new materials for high temperature applications.

Recently, Yamabe-Mitarai et al. [1–8] proposed and studied a new class of single crystal alloys namely refractory super alloys, based on high melting point fcc metals such as rhodium and iridium with $L1_2$ intermetallic compounds. They are found to have a micro structure similar to the commercial Nickel based super alloys. The mechanical properties of some of the rhodium based intermetallic compounds were studied by Miura et al. [9]. High pressure ab initio study of the electronic structure of the rhodium based and iridium based intermetallic compounds were studied by Rajagopalan et al. and Sundareswari et al. [10,11] respectively. The elastic properties of iridium and rhodium based intermetallic compounds were studied by Chen et al. [12,13]. In order to achieve excellent fatigue properties, the turbine blades should be made of materials of low thermal expansion and high thermal conductivity. Studies on rhodium based alloys, showed that they have low density, better oxidation resistance, lower thermal expansion, higher thermal conductivity [14] and high melting point (∼2450 °C), which make them serve as promising structural materials for ultra high temperature gas turbine applications. Having studied the band structure of rhodium based intermetallic compounds with V group and IV group transition metals, we intend to extend our study with the III group elements such as Sc, Y and La and try to compare their physical properties. To our knowledge, neither the experimental nor the theoretical study on Rh_3Sc, Rh_3Y and Rh_3La is available in the related literature. Hence the present study is focused on the intermetallic compounds namely, Rh_3Sc, Rh_3Y and Rh_3La, in order to throw more light on their electronic and physical properties by computing the band structure, density of states, bulk modulus, cohesive energy, etc. using the TB-LMTO method. It is believed that the results may be of interest to materials researchers.

[a] e-mail: mraja1948@yahoo.co.in

Table 1.

Compound/ Space group No.	Position of the atoms
Rh_3Sc (221)	Sc (0, 0, 0)
	Rh (0, 0.5, 0.5)
Rh_3Y (194)	Rh (0, 0, 0)
	Rh1 (0, 0, 0.25)
	Rh2 (0.333, 0.667, 0.75)
	Rh3 (0.8334, 0.6668, 0.1272)
	Y(0.333, 0.667, 0.25)
	Y1(0.333, 0.667, 0.0418)
Rh_3La (166)	Rh (0, 0, 0.5)
	Rh1(0, 0, 0.3344)
	Rh2(0.504, 0.496, 0.0818)
	La (0, 0, 0)
	La1 (0, 0, 0.1402)

2 Computational details

2.1 Structure aspects

It was reported experimentally [15,16] that Rh_3Sc crystallizes in Cu_3Au type (cubic) structure, Rh_3Y in $CeNi_3$type (hexagonal) structure, whereas Rh_3La to exist in two phases namely Be_3Nb type and $CeNi_3$ type structures The space group, experimental lattice parameters and position of the atoms of each compound, which are taken from the above mentioned work, are given in the Tables 1 and 2.

2.2 Methodology

In this work, the Tight Binding Linear Muffin Tin Orbital method [17–19] is employed to compute the electronic structure of the compounds Rh_3Sc, Rh_3Y and Rh_3La; here the Stuttgart code-lmto47l is applied to do the computations. The electronic structure and the total energies within the atomic sphere approximation (ASA) are obtained in a manner similar to our earlier work [20]. In the atomic sphere approximation [21,22], the crystal is divided into space filling spheres centered on each of the atomic sites. Also combined corrections are included in it, which account for the non-spherical shape of the atomic spheres and the truncation of the higher partial waves inside the spheres, to minimize the errors in the LMTO method. The Wigner-Seitz sphere radii are chosen in such a way that the sphere boundary potential is minimum, and the charge flow between the two atoms is in accordance with the electro negativity criteria. The s, p, d and f partial waves are included in the computation. The exchange correlation potential within the local density approximation (LDA) is calculated using the parameterization scheme of von Barth and Hedin [23]. All important relativistic corrections except spin-orbit coupling are included. The tetrahedron method was used to calculate the density of states (DOS) [24]. The E and K convergence are also checked.

The total energies of Rh_3Sc, Rh_3Y and Rh_3La are calculated by reducing the cell volume. For the non-cubic structures, the experimental c/a ratio is used in all our calculations. The accuracy of total energies obtained within the density functional theory is sufficient to predict which structure at a given pressure has the lowest free energy [25]. The computed total energies for each of these compounds are fitted to the Birch equation of state [26], to obtain the pressure volume relation and the enthalpy values. The bulk modulus (B_0) is obtained using the relation,

$$B_0 = -V_0 \frac{dP}{dV}.$$

The theoretically calculated equilibrium lattice parameter and bulk moduli of each of these compounds are presented in the Table 2 and are compared with the available experimental data. It was found that there is a good agreement between them. From table, one can observe that the error in the calculated values of the lattice parameters vary from a minimum of 0.9% to a maximum of 1.7%. The experimental lattice parameters are calculated at room temperature, whereas the calculations are done at 0 K. Hence one can expect such deviation in the calculated lattice parameter values.

Further, from the fitted values, the enthalpy and pressure values are also noted for both the structures of the given compound between which a structural transition is expected. Graphs are drawn between the values of enthalpy and pressure, in Rh_3Y and Rh_3La, each for cubic and hexagonal structures of the given compound and are shown in Figures 1 and 2. From the graphs, it is understood that the enthalpy of both the structures of the given compound remain the same at one particular pressure, namely the transition pressure and is found to be about 108 kbar for Rh_3Y and 187 kbar for Rh_3La.

3 Results and discussions

3.1 Total energy and the nearest neighbour distance calculations

The total energies of Rh_3Sc in the cubic structure, Rh_3Y in the hexagonal structure and Rh_3La in hexagonal and rhombohedral structures are calculated by reducing the cell volume and are plotted as shown in the Figures 3(a–d). Except Rh_3Y and Rh_3La, the other similar rhodium based Rh_3X intermetallic compounds (where X = Ti, Zr, Hf, Nb, Ta and Sc) are reported experimentally to stabilize in $AuCu_3$ type structure [15]. Hence, we have examined whether the compounds namely Rh_3Y and Rh_3La, will undergo a structural phase transition to cubic structure under compression. The variation in total energy of cubic Rh_3Y and Rh_3La are shown in the Figures 3b and 3c along with that of their hexagonal phase. From the Figures 3b and 3c, it is clear that, a phase transition from hexagonal to cubic structure occurs in Rh_3Y and Rh_3La, which is predicted to be about 108 kbar and 187 kbar respectively for Rh_3Y and Rh_3La (refer Figs. 1, 2). To analyze further, the nearest neighbour distance is calculated, under compression, in both the compounds namely Rh_3Y and Rh_3La, for $CeNi_3$ type structure and for cubic structure (refer Tabs. 3 and 4). From the tables, one can observe that in each of the compounds, the nearest neighbour distance decreases with compression, for both the structures.

Table 2. Bulk Modulus (B_0) is obtained from the fit of total energy to the Birch equation of state.

Compound	Lattice parameter (au)		Bulk Modulus (B_0) (Mbar)
	Expt.	Calculated (present)	
Rh_3Sc-(Cubic)	$a = 7.371$	$a = 7.301$	2.331
Rh_3Y-(Hexagonal)	$a = 9.887$	$a = 9.723$	2.155
	$c = 32.854$	$c = 32.311$	
Rh_3La-(Hexagonal)	$a = 10.029$	$a = 9.956$	1.7382
	$c = 33.253$	$c = 33.011$	
Rh_3La-(Rhombohedral)	$a = 10.068$	$a = 9.974$	1.7385
	$c = 50.019$	$c = 49.549$	

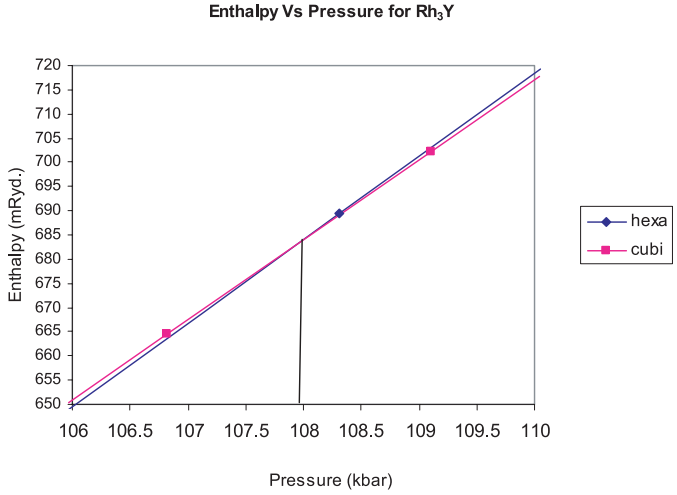

Fig. 1.

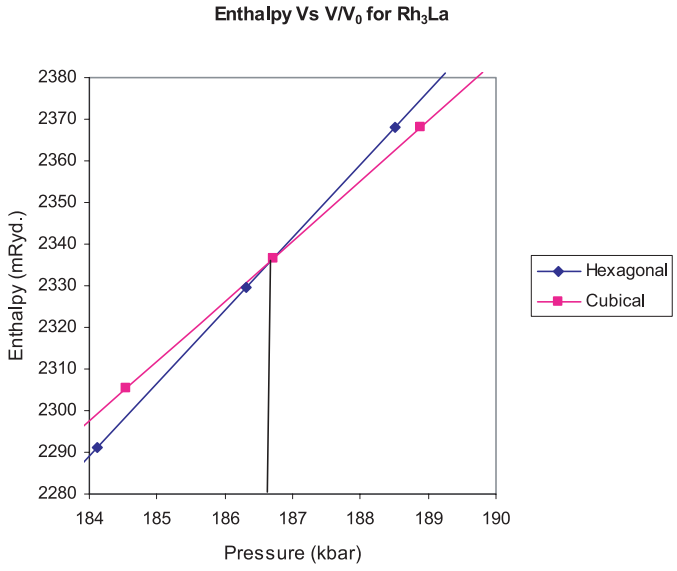

Fig. 2.

In the case of Rh_3Y, at $V/V_0 = 0.85$ (which corresponds to a pressure of about 108 kbar, at which the transition is predicted) and in Rh_3La, at $V/V_0 = 0.8$ (which corresponds to a pressure of about 187 kbar, at which the transition is predicted) the value of nearest neighbour distance is found to be 5.18 au (for Rh_3Y) and 5.15 au (for Rh_3La).

Table 3.

V/V_0	Nearest neighbour distance (au) in Rh_3Y at various compressions	
	Cubic	Hexagonal
1.0	5.472	5.871
0.95	5.380	5.771
0.90	5.284	5.668
0.85	5.184	5.561
0.80	5.080	5.450
0.75	4.972	5.334
0.7	4.859	5.213

Table 4.

V/V_0	Nearest neighbour distance (au) in Rh_3La at various compressions	
	Cubic	Hexagonal
1.0	5.547	5.980
0.95	5.453	5.878
0.90	5.356	5.773
0.85	5.255	5.664
0.80	5.150	5.550

These values are very close to the nearest neighbour distance value, in which the other Rh_3X compounds (where X = Ti, Zr, Hf, V, Nb, Ta and Sc) crystallize in the cubic phase at ambient condition (refer Tab. 5). This may be one of the reasons why the compounds Rh_3Y and Rh_3La prefer to undergo transition from hexagonal to cubic phase, each at the above mentioned compression, when their corresponding nearest neighbor distance values lie closer to that of the other Rh_3X compounds (where X = Ti, Zr, Hf, V, Nb, Ta and Sc) which are found to crystallize in the cubic phase at ambient condition.

The total energy variation of Rh_3La for the two experimentally reported structures, namely $CeNi_3$ type (hexagonal) and Be_3Nb type (rhombohedral) are shown in the Figure 3d. From this plot, we conclude that at ambient, the hexagonal phase is energetically more stable than the other phase. It was found that the energy difference between these two phases is about 32.7 mRyd.

To conclude, it can be stated that there is no possibility for the compounds Rh_3Y and Rh_3La to exist in cubic structure, at ambient condition, because of the following reasons (i) the nearest neighbour distance values at ambient condition in the cubic structures of Rh_3Y and Rh_3La (5.31 au and 5.34 au respectively) are not close to

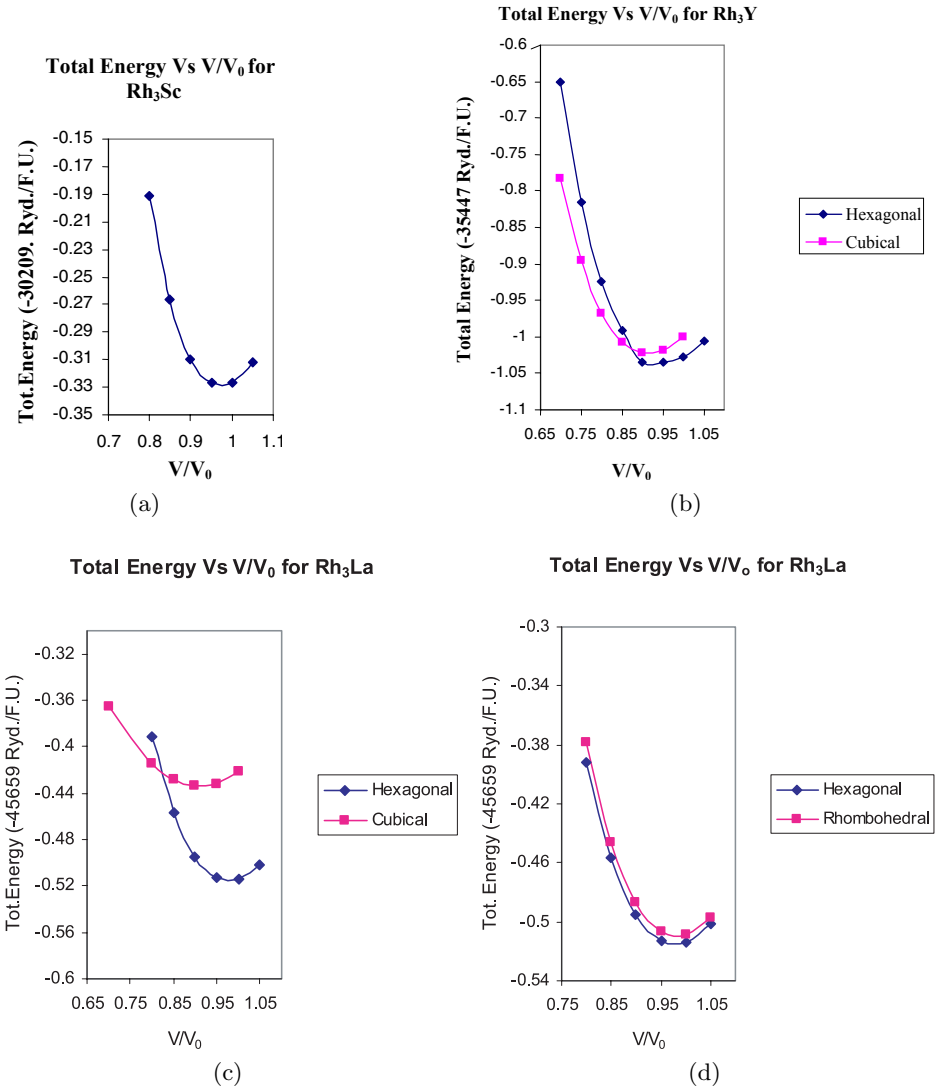

Fig. 3.

Table 5.

Compound (Cubic)	Nearest neighbour distance (au) at ambient condition
Rh_3Ti	5.070
Rh_3Zr	5.202
Rh_3Hf	5.195
Rh_3V	5.010
Rh_3Nb	5.121
Rh_3Ta	5.127
Rh_3Sc	5.163
Rh_3Y	5.311*
Rh_3La	5.338*

*Data obtained from the theoretically generated lattice parameter of the given compound.

the value in which the other Rh_3X compounds stabilize in cubic structure (refer Tab. 5); (ii). the nearest neighbour distance values for $CeNi_3$ type structures of Rh_3Y and Rh_3La (5.77 au and 5.94 au respectively) are found to be too large for a compound to crystallize in cubic structure.

3.2 Band structure calculations and density of states

The self-consistent band structure of Rh_3Sc (cubic), Rh_3Y and Rh_3La (in hexagonal phase) compounds at ambient condition are obtained using the TB-LMTO method along the higher symmetry directions and are shown in the Figures 4 to 7. In Rh_3Sc, the lowest lying bands around -0.4 Ryd. are due to Rh-s and Sc-s like electrons. The bands just above are the bands due to Rh-p and Sc-p like electrons. The bands around -0.26 Ryd. are due to Rh-d and Sc-d like electrons. The band profile of Rh_3Y and Rh_3La are found to be similar, except in Rh_3La, where, along M to G, K to M and L to H, the bands due to Rh-d like electrons are found to oscillate under pressure at the Fermi level and are explained as follows. The band profile of Rh_3La for three compressions, namely 0.9 V_0, 0.8 V_0 and 0.75 V_0 are shown in Figures 7a to 7c. At ambient condition, (Fig. 6), the Rh-d band, at G just touches the

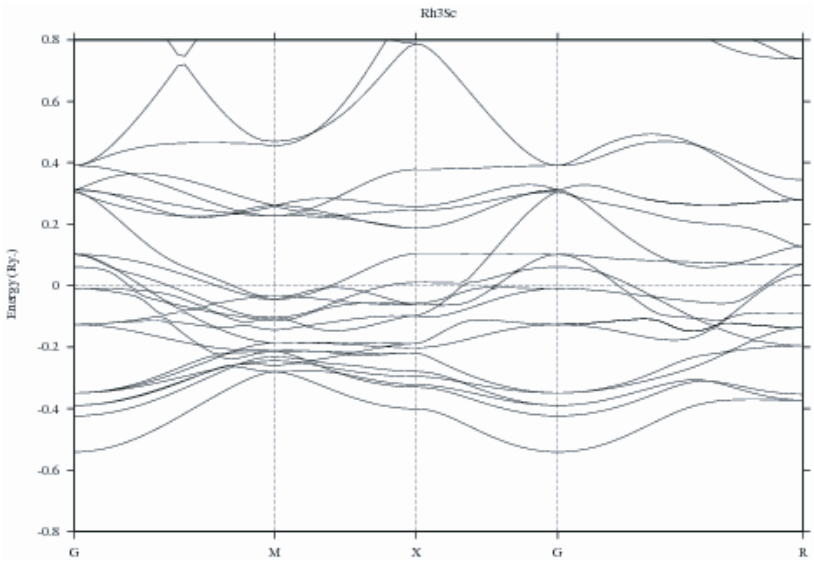

Fig. 4. Band structure of Rh_3Sc.

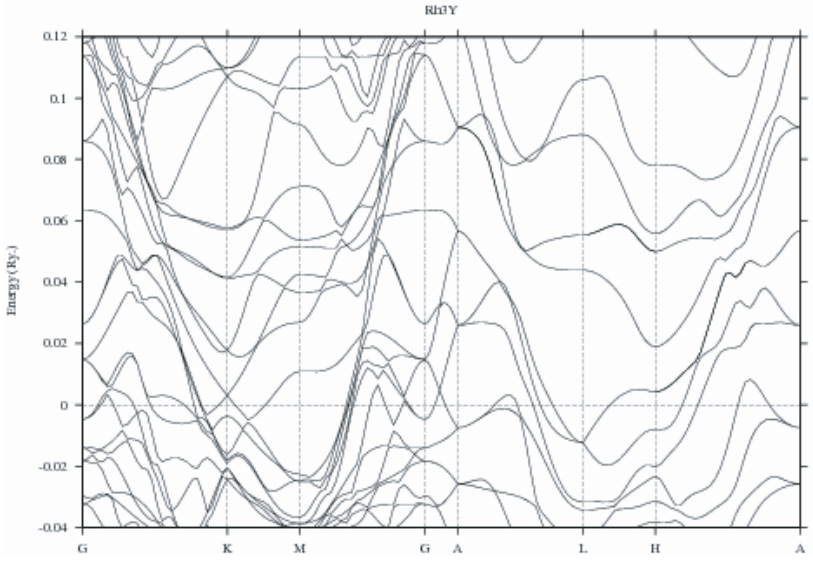

Fig. 5. Band structure of Rh_3Y.

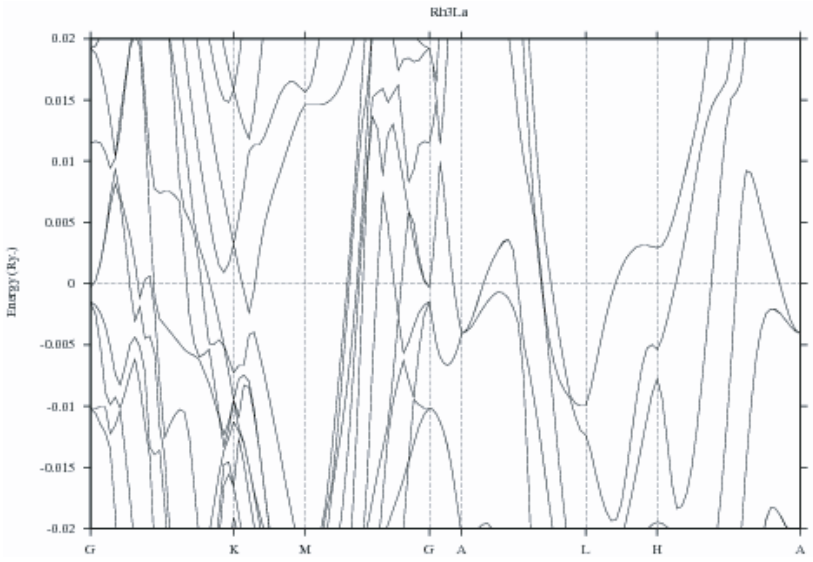

Fig. 6. Band structure of Rh_3La at ambient condition.

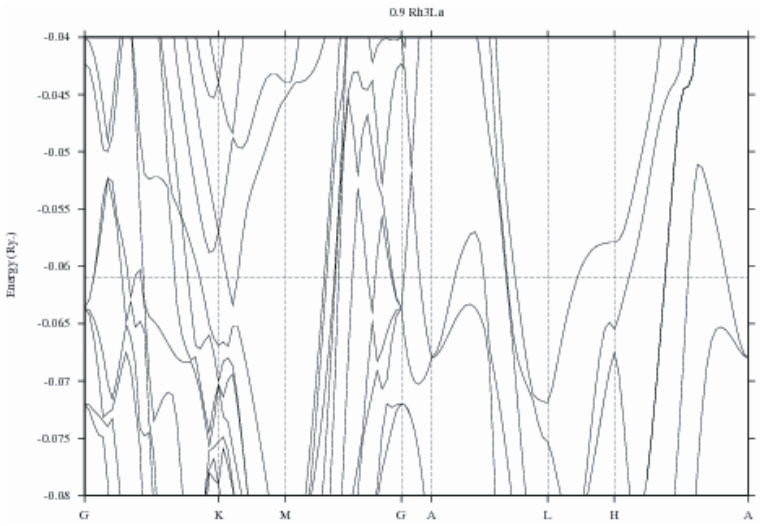

(a)

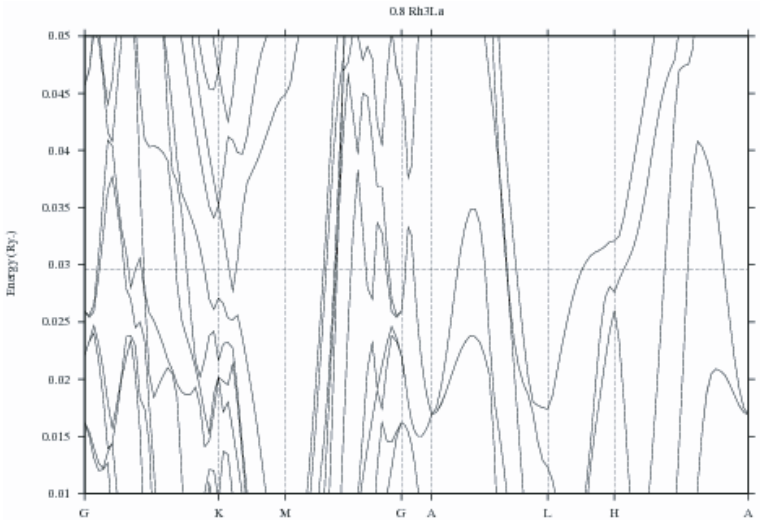

(b)

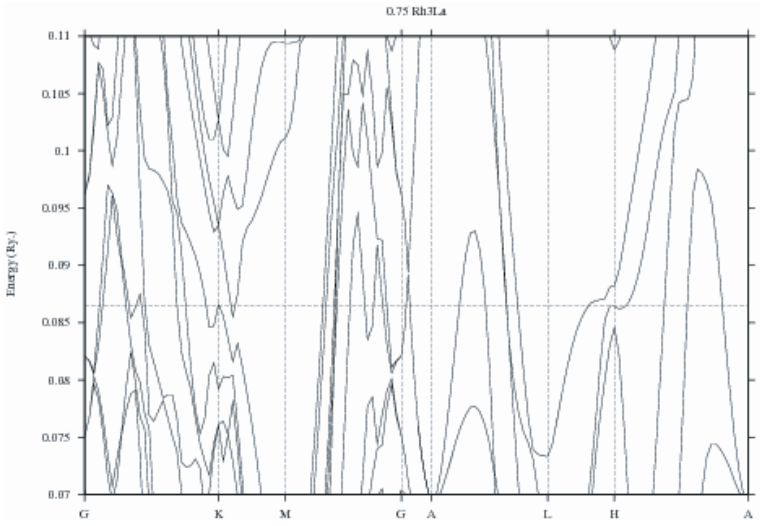

(c)

Fig. 7. (a) Band structure of Rh_3La at $V/V_0 = 0.9$. (b) Band structure of Rh_3La at $V/V_0 = 0.8$. (c) Band structure of Rh_3La at $V/V0 = 0.75$.

Table 6.

Compound	$N(E_f)$ (States/Ryd/cell)	Elect. Sp. heat Co-efficient (γ) (mJ/mol k^2)	Cohesive energy (eV/FU)
Rh_3Sc-(Cubic)	49.778	8.623	–42.349
Rh_3Y-(Hexagonal)	39.395	6.825	–34.106
Rh_3La-(Hexagonal)	34.470	5.972	–34.000
Rh3La-(Rhombohedral)	32.230	5.584	–33.920

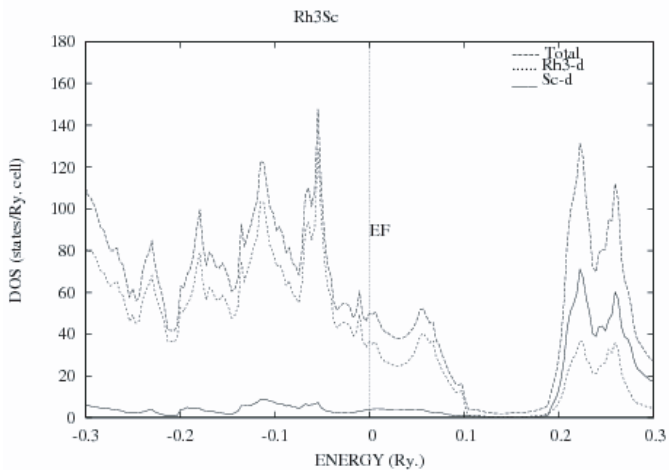

Fig. 8. Total and partial density of states of Rh_3Sc.

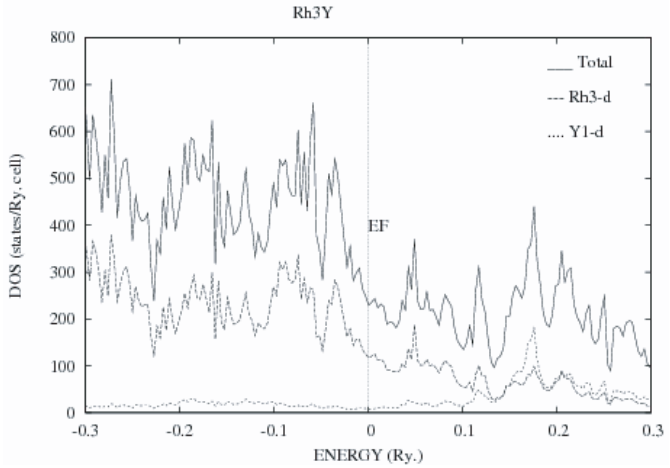

Fig. 9. Total and partial density of states of Rh_3Y.

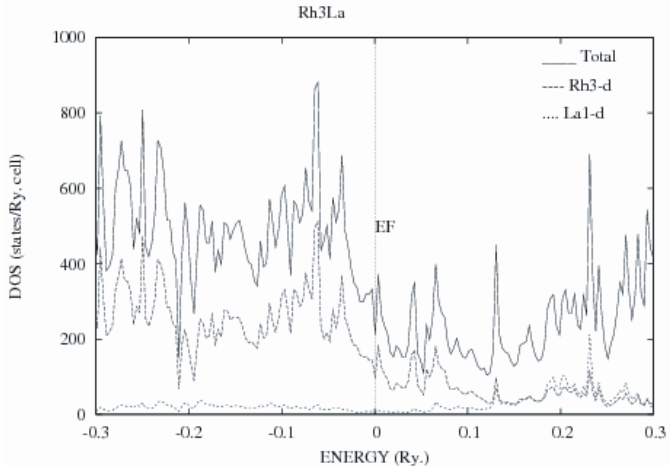

Fig. 10. Total and partial density of states of Rh_3La.

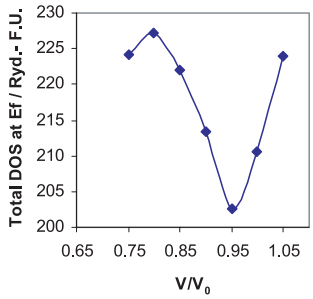

Fig. 11. Variation of total density of states at E_f with compression for Rh_3La.

Fermi level and further compressions (Figs. 7a to 7c) show that at G and along M to G, the band crosses the Fermi level and moves into the Fermi level. Further, along K to M and L to H, the bands are found to move up and at $V/V_0 = 0.75$ they tend to touch the Fermi level along L to H. Since some of the Rh-d bands cross the Fermi level during compression, it may change the Fermi surface topology of this compound.

The total and partial DOS of each of Rh_3Sc, Rh_3Y and Rh_3La compounds are shown in the Figures 8 to 10. In the histograms, the peaks of total DOS that lie below the Fermi level are mainly due to Rh-d like electrons. Since in Rh_3La, some of the bands cross the Fermi level under compression, there may be an electronic topological transition or Lifshitz type of transition [27] where it may also influence the monotonic variation of DOS at E_f. Physical properties such as electronic specific heat coefficient that involve the DOS at E_f, may get altered during compression due to such variation in the DOS. Figure 11 shows such variation of total density of states at E_f with compression for Rh_3La. The total density of states at E_f decreases continuously with pressure till $V/V_0 = 0.95$ and further compression leads to increase in the DOS at E_f and reaches a maximum at $V/V_0 = 0.8$ and decreases on further compression. A similar behaviour was observed by Rajagopalan et al for phosphorus [28], by Chu et al for rhenium [29], by Makarow et al for thallium [30] and by

Sahu et al for $CeAl_2$ [31]. Further, this kind of electronic topological transition may be used suitably to improve the thermo electric properties of certain materials [32].

3.3 Bulk modulus and cohesive energy calculation

The calculated bulk moduli values of each of the compounds Rh_3Sc, Rh_3Y and Rh_3La are listed in Table 2, from which it is noticed that the bulk moduli value decreases as one goes from Rh_3Sc to Rh_3La. The same trend is also seen in the bulk moduli values of the elemental solids namely Sc, Y and La [33]. In general, the bulk modulus could be used as a measure of the average bond strengths of atoms of the given crystal [34]. Then one can say that the average bond strength of Rh_3Sc is more compared to Rh_3Y and Rh_3La. A similar study for Ir_3X and Rh_3X (where X = Ti, Zr, Hf, V, Nb, Ta) intermetallic compounds are reported recently by Kuiying Chen et al. [13,14]. The bulk moduli values reported by us [11,12] for Ir_3X and Rh_3X intermetallic compounds find good agreement with these values.

It is known that the cohesive energy (E_{coh}) is the difference between the free atom energy and the crystal energy. For each of the compounds, Rh_3Sc, $Rh_3Y$and Rh_3La, the cohesive energy is calculated as follows: the total energy is obtained by solving semi — relativistic Schrödinger equation, first for the given compound and then for the free atom. The difference between them gives the cohesive energy of the given compound. In the present work, the cohesive energies are calculated for one formula unit; one formula unit consists of four atoms. The cohesive energy values of Rh_3Sc, Rh_3Y and Rh_3La are tabulated in the Table 6. The E_{coh} of rhodium, scandium, yttrium and lanthanum are found to be 5.75, 3.9, 4.37 and 4.47 in ev/atom respectively [33]. One can compare the cohesive energy values of the compounds with that of its constituent atoms. A similar comparison is reported for PtN by Jamal Uddin et al. [35]. The cohesive energy of Rh_3La, in rhombohedral and hexagonal structures are calculated and are given in Table 6, from which it can be said that, the hexagonal Rh_3La is more stable than rhombohedral Rh_3La.

Further, at transition (where $V/V_0 = 0.8$), the cohesive energy of Rh_3La is calculated for both cubic (2.40 Ryd/FU) and hexagonal structure (2.38 Ryd/FU) from which it is clear that cubic structure is more stable than hexagonal structure at the transition.

3.4 Electronic specific heat coefficient

At temperatures, much below the Debye temperature, the specific heat capacity of material is given as the sum of the electronic and lattice contribution [33], viz. $C = \gamma T + AT^3$, where γT represents the electronic contribution, AT^3 represents the lattice contribution and γ represents the electronic specific heat coefficient. The electronic specific heat coefficient (γ_{th}) for each of Rh_3Sc (cubic), Rh_3Y and Rh_3La (hexagonal) compounds is calculated at ambient conditions using the expression,

$$\gamma_{th} = \pi^2 \, k_B^2 \, N(E_f)/3,$$

where $N(E_f)$ represents the density of states at the Fermi level and k_B is the Boltzmann constant. For lack of experimental data, the present results are not compared. If experimental results for γ are available, one can estimate the electron-phonon mass enhancement factor (λ) using the expression,

$$.\gamma_{exp}. = \gamma_{th.}(1 + \lambda).$$

The electronic specific heat coefficient of Rh_3Sc, Rh_3Y and Rh_3La are calculated and tabulated in Table 6.

4 Conclusion

Systematic Tight Binding Linear Muffin Tin Orbital (TB-LMTO) calculations have been performed on the intermetallic compounds such as Rh_3Sc, $Rh_3Y$and Rh_3La as a function of reduced volume. The theoretically calculated equilibrium lattice parameter of each of these compounds is found to agree with the experimental values. The theoretically arrived bulk moduli values of these compounds shows that the bulk modulus and hence the average bond strength decreases from Rh_3Sc to Rh_3La. In other words, it follows the same trend as that of the elemental solids namely scandium, yttrium and lanthanum. A phase transition is predicted for Rh_3Y and Rh_3La, from hexagonal to cubic structure at a pressure of about 108 kbar and 187 kbar respectively. Of the two experimentally reported structures of Rh_3La, namely $CeNi_3$ type and Be_3Nb type, at ambient condition, the $CeNi_3$ type hexagonal structure is found to be more stable than the other. It is because the cohesive energy is more (and total energy is minimum) for $CeNi_3$ type hexagonal structure. It is clear from the above study that for hexagonal Rh_3La, under pressure, the Fermi surface topology can be changed, since some of the Rh-d bands cross the Fermi level under compression. A change in the Fermi surface topology then lead to some changes in the physical and thermo dynamical properties of Rh_3La under pressure. The change in the Fermi surface topology of Rh_3La is reflected in the total density of states at E_f, which leads to a Lifshitz type of transition. From the computed partial number of electrons at different sites, it is found that, under pressure, there is a continuous transfer of d-like states from A (Rh)-site to B (Sc, Y and La)-site, which may trigger a structural phase transition, and change the nature of chemical bonding in these compounds.) Therefore it is suggested to perform high-pressure X-ray diffraction studies of these compounds, to determine the phase stability, the nature of the chemical bonding of these compounds and also to verify the bulk moduli values of these compounds. It is also suggested to measure the electronic specific heat coefficient of these compounds to determine the electron-phonon mass enhancement factor.

References

1. Y. Yamabe-Mitarai, Y. Koizumi, H. Murakami, Y. Ro, T. Maruko, H. Harada, Scripta Metall **35**, 211 (1996)
2. Y. Yamabe-Mitarai, Y. Ro, T. Maruko, H. Harada, Metall Mater Trans. A **29**, 537 (1998)
3. Y. Yamabe-Mitarai, S. Nakazawa, H. Harada, Scripta Metall **43**, 1059 (2000)
4. Y.F. Gu, Y. Yamabe-Mitarai, Y. Ro, T. Yokokawa, H. Harada, Scripta Metall. **40**, 1313 (1999)
5. Y. Yamabe-Mitarai, S. Nakazawa, H. Harada, Solid Mech. Mater. Eng. **45**, 1 (2002)
6. Y. Yamabe-Mitarai, Y. Ro., T. Maruko, T. Yokokawa, H. Harada, Structural Intermetallics, TMS, 805 (1997)
7. Y. Yamabe-Mitarai, Y. Koizumi, H. Murakami, Y. Ro, T. Maruko, H. Harada, Scripta Mat. **36**, 393 (1997)
8. Y. Yamabe-Mitarai, M.H. Hong, Y. Ro, H. Harada, Phill. Mag. Lett. **79**, 673 (1999)
9. S. Miura, K. Honma, Y. Terada, J.M. Sanchez, T. Mohri, Intermetallics **8**, 785 (2000)
10. M. Rajagopalan, M. Sundareswari, J. Alloys and Comp. **379**, 8 (2004)
11. M. Sundareswari, M. Rajagopalan, Int. J. Mod. Phys. B **19**, 4587 (2005) (World Scientific Publishing Company)
12. K. Chen, L.R. Zhao, J.S. Tse, J. Appl. Phys. **93**, 2414 (2003)
13. K. Chen, L.R. Zhao, J.S. Tse, J.R. Rodgers, Phys. Lett. A **331**, 400 (2004)
14. Y. Terada, K. Ohkubo, S. Miura, J.M. Sanchez, T. Mohri, J. Alloys Comp. **354**, 202 (2003)
15. P. Villars, L.D. Calvert, *Pearson's Handbook of Crystallographic Data for Intermetallic Phases* (ASM International, Metals Park, OH, 1985)
16. Singh, Raman, Trans. Met. Soc. AIME **245**, 1561 (1969)
17. O.K. Andersen, O. Jepsen, Phy. Rev. Lett. **53**, 2571 (1984)
18. O.K. Andersen, Z. Pawlowska, O. Jepsen, Phy. Rev. B **34**, 5253 (1986)
19. H.J. Nowak, O.K. Andersen, T. Fujiwara, O. Jepsen, P. Vargas, Phys. Rev. B **44**, 3577 (1991)
20. Sk. Khadeer Pasha, M. Sundareswari, M. Rajagopalan, Physica B **348**, 1-4, 206 May (2004)
21. O.K. Andersen, Phys. Rev. B. **12**, 3060 (1975)
22. H.L. Skriver, *The LMTO Method* (Springer, Heidelberg, 1984)
23. U. von Barth, L. Hedin, J. Phys. C **5**, 1629 (1972)
24. O. Jepsen, O.K. Andersen, Solid State Communications **9**, 1763 (1971)
25. N.E. Christensen, D.L. Novikou, R.E. Alonso, C.O. Rodriguez, Phys. Stat. Solidi (b) **211**, 5 (1999)
26. F. Birch, J. Geophys. Rev. **83**, 1257 (1978)
27. I.M. Lifshitz, Sov. Phys. JETP **11**, 1130 (1960)
28. M. Rajagopalan, M. Alouani, N.E. Christensen, J. Low Temp. Physics **75**, 1 (1989)
29. C.W. Chu, T.F. Smith, W.E. Gardner, Phys. Rev. B **1**, 214 (1970)
30. V.I. Makarow, V.G. Barlyakhtar, Sov. Phys. JETP **21**, 1151 (1965)
31. P.Ch. Sahu, N.V. Chandra Shekar, Pramana **54**, 685 (2000)
32. N.V. Chandra Shekar, D.A. Polvani, J.F. Meng, J.V. Badding, *Advances in High pressure Science and Technology*, edited by A.K. Bandyopadhyay, D. Varandani, K. Lal (National Physics Laboratory, New Delhi, 2001) pp. 310–314
33. Charles Kittel, *Introduction to Solid state physics*, 7th edn. (John Wiley & Sons, Inc. 1996)
34. D.G. Cierc, H.M. Ledbetter, J. Phys. Chem. Solids **59**, 1071 (1998)
35. J. Uddin, G.E. Scuscria, Phys. Rev. B **72**, 035101 (2005)